Recent water mass changes reveal mechanisms of ocean warming

Jan D. Zika*

School of Mathematics and Statistics, University of New South Wales, Sydney, Australia

Jonathan M. Gregory

National Centre for Atmospheric Science, University of Reading, Reading, UK

Elaine L. McDonagh

NORCE, Norwegian Research Centre, Bjerknes Centre for Climate Research, Bergen, Norway

and

National Oceanography Centre, Southampton, UK

Alice Marzocchi and Louis Clement

National Oceanography Centre, Southampton, UK

Corresponding author: Jan D. Zika, j.zika@unsw.edu.au

ABSTRACT

Over 90% of the build up of additional heat in the earth system over recent decades is contained in the ocean. Since 2006 new observational programs have revealed heterogeneous patterns of ocean heat content change. It is unclear how much of this heterogeneity is due to heat being added to and mixed within the ocean leading to material changes in water mass properties or due to changes in circulation which redistribute existing water masses. Here we present a novel diagnosis of the 'material' and 'redistributed' contributions to regional heat content change between 2006 and 2017 based on water mass theory. We show that material warming has large spatial coherence. The material change tends to be smaller than the redistributed change at any geographical location, however it sums globally to the net warming of the ocean, while the redistributed component sums, by design, to zero. Material warming is robust over the time period of this analysis, whereas the redistributed signal only emerges from the variability in a few regions. In the North Atlantic, water mass changes indicate substantial material warming while redistribution cools the subpolar region due to a slowdown in the Meridional Overturning Circulation. Warming in the Southern Ocean is explained by material warming and by anomalous southward heat transport of 118 ± 50 PW due to redistribution. Our results suggest near term projections of ocean heat content change and therefore sea level change will hinge on understanding and predicting changes in ocean redistribution.

1. Introduction

Over the past 50 years, as atmospheric greenhouse gas concentrations have increased, the ocean has absorbed more than ten times as much heat as all other components of the climate system combined (Rhein et al. 2013). This warming showed substantial spatial variability between 1993 and 2005, being up to ten times greater in some regions than the global average (Zhang and Church 2012). It is unclear whether this variability is due to geographical variation in the interior propagation of surface warming versus redistribution of existing heat within the ocean.

Ocean warming is an important issue because ocean thermal expansion is the largest projected contribution to global mean sea level rise in the 21st century (Church et al. 2013). Numerical climate models disagree on the pattern and amplitude of ocean heat content (OHC) change and hence sea level rise under anthropogenic greenhouse warming (Gregory et al. 2016). Understanding how heat has been taken up and redistributed by the ocean is essential for predicting future changes.

Mesoscale eddies and planetary wave processes drive variability in ocean temperature at 10-100km spatial scales and typically dominate differences between ship based observations spaced years apart. Most striking of these is the El Niño Southern Oscillation which lifts the thermocline in the western Pacific and lowers it in the east leading to an exchange of heat between shallow and deep layers. This oscillation dominates observed global mean temperature variability (Roemmich and Gilson 2011).

Numerical ocean models forced with historical atmospheric conditions have proved to be useful tools in quantifying the role of atmospheric forcing in setting regional variability in OHC (Drijfhout et al. 2014) and sea level (Penduff et al. 2011). However such models can be ineffective in simulating underlying climate change due to model drift and inaccuracies in model forcing, particularly global mean heat fluxes (Griffies et al. 2009). On the other hand coupled ocean atmosphere climate

models are routinely used to capture the effect of climate forcing. But such models only accurately simulate past unforced variability in regional OHC when, by chance, their internal variability is in phase with the observed system.

An advancement in terms of numerical ocean climate modeling has been the separation of OHC change into an 'added' and a 'redistributed' component in climate model simulations, where the former is due to change in the surface heat flux, and the latter due to rearrangement of existing OHC because of altered ocean heat transports (Banks and Gregory 2006). This decomposition is analogous to the 'anthropogenic' and 'natural' decomposition, that has revolutionized our understanding of oceanic carbon records (Khatiwala et al. 2013). Here we will present a novel method to diagnose the 'material' component of OHC change which we will show is closely related the 'added' component introduced by Banks and Gregory (2006).

Recent work has aimed to reconstruct the drivers of OHC change based on observationally derived air-sea boundary conditions. Zanna et al. (2019) for example used surface temperature anomalies combined with a tracer based approach to reconstruct the role of anomalous surface heat fluxes in centennial heat content change. Roberts et al. (2017) estimated the contribution of air-sea heat flux changes in setting mixed layer and depth integrated OHC budget over recent decades and inferred the role of ocean circulation as a residual. Here we aim to circumvent reliance on such boundary conditions and infer the mechanisms of ocean heat content change directly based on water mass changes.

Water mass based methods have been used to decompose local temperature and salinity changes into a dynamic 'heave' components and apparently material effects at constant density based on a one dimensional view of the water column (Bindoff and McDougall 1994). However broader scale horizontal motions influence ocean temperature on longer timescales and indeed vertical heaving does not directly affect regional depth integrated OHC.

In the present work we present a new method based on water mass theory with which we estimate recent drivers of three dimensional OHC change. In Section 2 we will review water mass theory and establish the relationship between changes in water masses as defined by their temperature and salinity and material changes in sea water temperature. We will describe in Section 3 how this theory is translated into a practical method to estimate material changes in water masses and map these into geographical space. We present results of an application of this method to recent data over the Argo period in Section 4. We discuss the results and compare them with existing work in Section 5 and give conclusions in Section 6.

2. Theory

Water mass analysis has long been used in physical oceanography to trace the origin of waters (Montgomery 1958). In the latter half of the 20th century a quantitative framework emerged to describe the relationship between water masses, air sea fluxes and mixing (Walin 1982). (See the review by Groeskamp et al. (2019).) Recent work has seen this framework advanced in two ways specifically relevant to our work here: to multiple tracer dimensions to understand the thermodynamics of ocean circulation (Nycander et al. 2007; Zika et al. 2012; Döös et al. 2012; Groeskamp et al. 2014; Hieronymus et al. 2014) and to unsteady problems to understand the ocean's role in transient climate change (Palmer and Haines 2009; Evans et al. 2014; Zika et al. 2015a,b; Evans et al. 2017, 2018).

An example of the utility of the water mass transformation framework in understanding transient change is provided by Zika et al. (2015a). The distribution of water in salinity coordinates is influenced by the water cycle and turbulent mixing, the latter only being able to collapse the range of salinities the ocean covers. This means that changes in the width of the salinity distribution indicate an enhancement of the water cycle and/or a reduction in that rate at which salt is mixed. In

this project we extend this concept to consider how changes in the temperature-salinity distribution relate to material changes in water masses.

Material changes in conservative temperature (here after T) following the motion of an incompressible fluid are related to Eulerian changes and advection by

$$\frac{DT}{Dt} = \frac{\partial T}{\partial t} + \mathbf{u} \cdot \nabla T \tag{1}$$

where $\mathbf{u}$ is the 3D velocity vector and $\frac{DT}{Dt}$ is the material derivative which is related to sources and sinks of heat and irreversible mixing.

Even if a perfect record of perfect record of $\frac{\partial T}{\partial t}$ were available at a fixed location, (1) does not give information regarding the relative roles of advection ($\mathbf{u} \cdot \nabla T$) and material processes ($\frac{DT}{Dt}$). We therefore consider the water mass perspective as an alternative to the Eulerian perspective. The following theory draws directly from Hieronymus et al. (2014).

We characterize water masses by their T and absolute salinity (here after S). The volume of water per unit T and S at $T = T^*$ and $S = S^*$ is

$$v(T^*, S^*) = \frac{\partial^2}{\partial T \partial S} \int_{T<T^*, S<S^*} dV. \tag{2}$$

Considering all the water in the climate system and retaining the incompressibility assumption, the only way v can change is via 'transformation'. That is, by making water parcels warmer, colder, saltier or fresher. This realization permits the following continuity equation

$$\frac{\partial v}{\partial t} + \frac{\partial}{\partial T}\left(v\dot{T}\right) + \frac{\partial}{\partial S}\left(v\dot{S}\right) = 0. \tag{3}$$

Here $\dot{T}$ is the average material derivative of T within a water mass. That is

$$\dot{T}(T^*, S^*) = \frac{1}{v}\frac{\partial^2}{\partial T \partial S} \int_{T<T^*, S<S^*} \frac{DT}{Dt} dV \tag{4}$$

and likewise $\dot{S}$ is the average material derivate of S.

In (3) the terms $v\dot{T}$ and $v\dot{S}$ are the transformation rates in the temperature and salinity directions respectively. Equation (3) states that the amount of water between two closely spaced isotherms (T and $T + \partial T$) and isohalines (S and $S + \partial T$) will go up, if more water it made warmer at T than at $T + \partial T$ and/or more water is made saltier at S than at $S + \partial S$ (i.e. more water comes in than goes out).

Here we will use changes in v to infer $\dot{T}$. This will allow us to estimate the material processes influencing ocean temperature change.

Note that although $\frac{DT}{Dt}$ is controlled purely by heat sources and sinks and mixing and not ocean circulation. Therefore advection has no role in water-mass (T–S) space, presuming it does no mixing, but this does not imply that it has no role in geographical space. Consider for example material warming which is detected within a deep water mass disconnected from the air-sea interface. Heat must have been mixed into that water mass but the heat may have been 'added' to the sea surface, advected to the deep water mass and then mixed into that water mass. In the Appendix we will indeed show that our water mass based material temperature change corresponds closely with simulated 'added temperature' in an ocean model where explicit anomalous heat fluxes are prescribed and the corresponding temperature anomaly is tracked as a tracer throughout the ocean.

3. Method

Observational estimates of T and S come from the Enact Ensemble (V4.0, here after EN4, Good et al. 2013) for each month between 2006 and 2017 inclusive. We split these data into two periods of time: an 'early' period between 2006 and 2011 inclusive and a 'late' between 2012 and 2017 inclusive. We then define a discrete set of water masses for each time period by splitting the ocean

into nine geographical regions and within each region by splitting the ocean up according to T–S bins.

Our nine geographical regions are defined: the Southern Ocean south of 35°S, the subtropical Pacific and Atlantic Oceans between 35°S and 10°S, the Indian Ocean north of 35°S, the tropical Pacific and Atlantic Oceans between 10°S and 10°N, the North Pacific north of 10°N, the Atlantic Ocean between 10°N and 40°N and the Atlantic and Arctic Ocean north of 40°N. To avoid discontinuities in our resulting analysis we transition linearly from one region to another over a 10° band (Figure 2).

We define T and S bin boundaries ($[T_{min}, T_{max}]$ and $[S_{min}, S_{max}]$ respectively) using a quadtree method. The quadtree method starts with a single (obviously oversized) bin with T boundaries [-6.4 °C, 96 °C] and S boundaries [-5.2g/kg, 46g/kg] in which the entirety of the ocean's sea water resides. The single bin is then split into 4 equally sized bins with the same aspect ratio as the original bin. The same process of splitting into four is repeated for any bin whose volume change is greater than a threshold of 62 x 10^{12}m^3 (equivalent to the volume of a 5° longitude by 5° latitude region at the equator with a depth of 200m) or until the bin size is 0.4 °C by 0.2g/kg. In the supplementary text we show that changing the size of these bins by a factor of two does not substantially change our results.

The quadtree method is applied within each region and for the change between the late and early periods. This results in bin edges defining 1447 water masses. These bins are then used to define both the 'early water masses' and the 'late water masses'.

The ith early water mass is described by its geographical region (from one to nine), its volume ($V1_i$), its volume weighted mean temperature ($T1_i$) and its volume weighted mean salinity ($S1_i$, Fig. 2). Likewise, the jth late water mass is described by its region, volume ($V2_j$), temperature ($T2_j$) and salinity ($S2_j$).

To change the water mass distribution from that of the early period to that of the late period requires that water be 'transformed' in T–S space. When water transforms it changes its T and S either in the same geographical region or as it moves to a region nearby. Transformation between early and late water masses is described by a matrix g. The ith column and jth row (g_{ij}) corresponds to the average transformation of water from early water mass i to late water mass j in units of m^3 s^{-1} over some time period Δt. Note that even if the ith water mass for the early period has the same temperature and salinity bounds as the ith water mass of the late period, the distribution of properties within the bin can change, so the average temperature and salinity of the water within the bin can change. That is, in general $T1_i \neq T2_i$ and $S2_i \neq S2_i$, so g_{ij} is always a 'transformation', even with $i = j$.

Since the total volume of water is conserved from the early to late periods the following volume budget is applied

$$V1_i = \Delta t \sum_{j=1}^{N} g_{ij} \text{ and } V2_j = \Delta t \sum_{i=1}^{N} g_{ij}. \tag{5}$$

Our goal is to estimate the matrix g. Out of the infinite number of choices which could satisfy (5), we find a 'minimum transformation', using an Earth Mover Distance (EMD) algorithm (Pele and Werman 2008, 2009). The EMD solves the hypothetical problem of moving earth from a set of mounds, each with varying amounts of earth, into a set of holes with varying amounts of empty space to be filled. The optimization problem is to find the smallest total mass weighted distance that needs to be travelled in order to empty the mounds and fill the holes. In our case the 'mounds' are the early water masses and the 'holes' are the late water masses.

For the EMD algorithm, we require a 'distance' metric (D), which is a matrix whose ith column and jth row (d_{ij}) is the cost of moving from the ith early water mass to the jth late water mass.

The EMD algorithm then estimates g such that (5) is satisfied and the following total transport weighted 'distance' travelled is minimized

$$\sum_{j=1}^{N}\sum_{i=1}^{N} g_{ij} d_{ij}. \tag{6}$$

We use the following distance metric

$$d_{ij} = (T1_i - T2_j)^2 + [a(S1_i - S2_j)]^2 + \delta_{ij} \tag{7}$$

where temperature and salinity differences are squared so that long trajectories in T–S space are penalized more than short ones and a is an arbitrary constant which scales the salinity change relative to the temperature change. The intent of δ_{ij} is to permit water masses to move across our arbitrary geographical boundaries without penalty but at the same time to stop direct exchange between geographically disconnected regions, for example between the Southern Ocean and Arctic or the tropical Atlantic and tropical Pacific. To achieve this we set $\delta_{ij} = 0$ where the ith and jth water masses are in the same or adjacent geographical regions and $\delta_{ij} = \infty$ otherwise. Regions which share a meridional boundary are considered adjacent. The Arctic and North Pacific are not considered adjacent while the Indian Ocean and equatorial Pacific regions are considered adjacent.

We choose the constant a to be the ratio of a typical haline contraction coefficient to a typical thermal expansion coefficient (a = β_0/α_0 = 4.28). This does not mean that transformations along density surfaces are necessarily preferred. The squares in (7) mean that density compensated changes in T and S are penalized as much as changes of the same magnitude where one of the signs is reversed. We have tested the sensitivity of the method to varying a by a factor of two and found only negligible changes in inferred warming (see the Appendix).

By moving water from a temperature $T1_i$ to $T2_j$, the transformation g_{ij} implies warming or cooling of a portion of the ith early water mass, transforming it into a portion of the jth late

water mass. To gain a picture of the net material change within a water mass we add up all the warming/cooling necessary to transform the ith early water mass into all of its destination water masses to derive an average material warming rate ($\dot{T}_i$) within each early water mass

$$\dot{T}_i = \frac{1}{V1_i} \sum_{j=1}^{N} (T2_j - T1_i) g_{ij}. \tag{8}$$

which is shown in Fig. S1.

We now aim to use $\dot{T}$ to define a 3D material temperature change variable $\Delta T_{Material}$. To do this we make the assumption that the warming of a particular water mass occurred evenly (in a volume and time weighted sense) over the regions and times during which that water mass existed in the early period. E.g. if a particular location was occupied by the nth water mass for the entire period 2006 to 2011, then the inferred rate of change of material temperature at that location would have been $\dot{T}_n$. Likewise, if the nth water mass occupied that location between 2006 and 2008 and the mth water mass existed there between 2009 and 2011, then the rate of change of material heat content will be $(\dot{T}_n + \dot{T}_m)/2)$. More precisely, at every location $\mathbf{x}$ we define $T_{Material}$ as

$$\Delta T_{Material}(\mathbf{x}) = \int_{t_1}^{t_2} \sum_{i=1}^{N} \Pi(T(\mathbf{x}), [T_i^{min}, T_i^{max}]) \Pi(S(\mathbf{x}), [S_i^{min}, S_i^{max}]) \dot{T}_i dt.$$

Above, Π is a boxcar function such that $\Pi(T, [T_1, T_2])$=1 when $T_1 \leq T < T_2$ and 0 otherwise and t_1 the start of 2006 and t_2 is the end of 2011.

We could equally have attributed warming to each late water mass based on how much heat was required to transform the early water masses into the late water mass. We find the above approach more intuitive. The difference between maps of material heat content change made using the two approaches are well within the uncertainties stated (not shown).

We will contrast the inferred material warming at $\mathbf{x}$ against the total warming $\Delta T(\mathbf{x}) = T(\mathbf{x}, t_2) - T(\mathbf{x}, t_1)$ with the residual of the two being a redistribution component such that

$$\Delta T_{Material} = \Delta T - \Delta T_{Redistribution} \tag{9}$$

In the Appendix we compare results of our method applied to synthetic data from a climate model simulation to an added heat variable explicitly simulated by the model. We find good agreement between added heat and our inferred $\Delta T_{Material}$ and between simulated redistributed heat and inferred $\Delta T_{Redistribution}$ when ocean temperature and salinity are fed in as 'data' to the method. The Appendix also explores sensitivity of our results to parameter choices. The uncertainties we place on OHC change are ± 2 standard deviations of a bootstrap ensemble, also described in the Appendix.

To produce maps of the total, material and redistributed contributions to the heat content we multiply the density and heat capacity of sea water by the respective temperature change and vertically integrate these through the entire water column. Our method also produces a material salinity change. We leave discussion of those data to future work.

4. Results

Patterns of total OHC change between early and late periods are heterogeneous (Fig. 3A). There are basin scale patches of decreasing heat content in the western equatorial and tropical Pacific, in the Pacific sector of the Southern Ocean, in the subtropical south Indian Ocean, and the subpolar North Atlantic. Warming is seen most strongly in the tropical eastern Pacific, south Atlantic Ocean and subtropical North Atlantic. These changes are highly sensitive to the specific observation years chosen and the length of the epochs reflecting the regional timescale of variability associated with the redistributed component. Uncertainty is far larger than the signal in the majority of regions

(stippling in Fig. 3A) and coincident with previously-identified regions of large sea level anomaly variability (Penduff et al. 2011). However, there are a few regions (e.g. the Southern Ocean and North Atlantic) where the regional redistributed signal is robust and emerges from the uncertainty (Fig. 3B).

Material heat content change shows a smaller amplitude but more coherent signal than redistributed heat (Figs. 3B and 3C). Material warming is seen across almost the entirety of the globe, with maxima in the Southern Hemisphere and Atlantic subtropical convergence zones (Maximenko et al. 2009), consistent with model simulations of passive ocean heat uptake due to anthropogenic greenhouse warming (Gregory et al. 2016). Strikingly however, the uncertainty in material heat content change is far smaller than that of total OHC change (stippling in Fig. 3C). This suggests that heat was added to and distributed within the ocean persistently over the Argo period and that this warming is not an artifact of a particularly warm year or years.

Zonally integrating the net OHC change reveals a signal of roughly the same magnitude as its uncertainty at all latitudes (Fig. 4A). Zonally integrated redistributed heat likewise has a small signal to uncertainty ratio except in the Southern Ocean (Fig. 4A). Accumulating the redistributed heat contribution from north to south gives the meridional heat transport due to redistribution. Broadly, heat is redistributed from north to south with a southward cross equatorial transport of 73 $\pm$ 60 TW between the two epochs (Fig. 4C).

Material heat content change is larger than its uncertainty at most latitudes and shows a peak at 35°S, 15°N and 35°N. The material heat content change peaks at 35°S and 35°N are collocated with climatological wind stress curl minima, which drive Ekman downwelling.

Table 1 shows material, redistributed and total heat content changes by ocean basin. Material heat content change is distributed among the Indian, South Pacific and South Atlantic basins approximately according to their area. However, the North Atlantic stores close to 25% of the

global ocean's material heat content change despite representing less than 12% of its area (Table 1). An outsized role for the Atlantic and Southern Ocean in storing material heat content change in the climate system has also been foreseen in numerical modeling studies (Lee et al. 2011; Kuhlbrodt and Gregory 2012).

We identify robust redistributed warming signals in the sub-tropical North Atlantic and Southern Ocean. Warming in the sub-tropical North Atlantic is compensated by cooling in the sub-polar North Atlantic consistent with a 40 ± 13 TW southward transport of heat across 44°N (Fig. 3C, Fig. 4C). Warming in the Southern Ocean is far larger and explained by 118 ± 50 PW of southward heat transport across 32°S.

5. Discussion

Recent anomalous southward heat transport in the North Atlantic has been well documented and has been attributed to a downturn in the Atlantic Meridional Overturning Circulation (Smeed et al. 2013; Bryden et al. 2020). Observed heat transport anomalies equate to a downturn in MHT equivalent to -23±60 TW for the period 2006-2011 vs 2012-2017 at 26°N in the Atlantic (see the Appendix for details of this calculation which is based on data from Bryden et al. 2020) which is consistent with our estimate of the change in redistribution heat transport of -23±19 TW (Fig. 4, uncertainties are ± 2 standard deviations).

The large apparent meridional heat transport we have identified in the Southern Ocean was previously identified by Roberts et al. (2017) based on the residual of observed OHC change and estimates of air sea heat fluxes. Their approach captures additional heat in the system where it is fluxed into the ocean while our approach estimates how that heat is distributed. Nonetheless, the correspondence between our results and theirs is reassuring and perhaps not surprising if the redistribution signal is large as both approaches indicate.

The approach of Zanna et al. (2019) is more directly comparable to ours. They reconstruct the passive contribution to ocean warming since 1850 by propagating SST anomalies into the ocean interior using Green's functions. They compare their inferred passive warming between 1955 and 2016 to the warming observed in situ and find evidence of a large southward redistribution of heat in the Northern Hemisphere. This may suggest that the southward redistribution of heat inferred by both Roberts et al. (2017) and this study in the Southern Hemisphere is a more recent occurrence.

6. Conclusions

In conclusion we have shown that:

- Water mass changes between 2006-2011 and 2012-2017 can be interpreted in terms of a material warming across the globe, concentrated most strongly in the Southern Ocean and North Atlantic, consistent with simulations of the addition of heat into the ocean due to green house forcing;
- The majority of the pattern of ocean heat content change over that period can be explained by a redistribution of existing water masses within the ocean;
- The inferred redistribution indicates a downturn in northward meridional heat transport into the sub-polar North Atlantic of 40 ± 13 TW and an anomalous southward heat transport into the Southern Ocean of 118 ± 50 TW.

The material warming signal we have inferred is generally weaker than redistribution, but the signal is far less sensitive to changes in the years over which the analysis was carried out. This suggests material warming may be giving a robust indication of slow thermodynamic changes in the ocean, potentially as a result of anthropogenic forcing. This would be remarkable since there are only 6 years between the centre of the early and late periods we have considered.

We expect the strength of the material warming signal to increase into the future as the ocean warms. However since the redistribution signal is so large, circulation changes and variability must be understood if near term regional sea level change is to be projected accurately.

Acknowledgments. We would like to acknowledge the UK Met Office's Hadley Centre for maintaining the EN4 data set used here and Professors O. Pele and M. Werman for developing and making available their Earth Mover Distance code. We thank John Church, Richard Sanders and Lijing Cheng for helpful suggestions regarding this manuscript.

JZ was supported by Australian Research Council Grant DP190101173. EM, AM and LC were supported by Natural Environment Research Council grant NE/P019293/1 (TICTOC) and EM was also supported by European Union Horizon 2020 grant 817578 (TRIATLAS). JG was supported by Natural Environment Research Council grants NE/P019099/1 (TICTOC) and NE/R000727/1 (UK-FAFMIP).

Data availability statement. Analyzed temperature and salinity data used in this study was from EN4 (Good et al. 2013) and is publicly available at https://www.metoffice.gov.uk/hadobs/en4/download-en4-2-1.html.

Code used to convert EN4 in-situ temperature and practical salinity fields to conservative temperature and absolute salinity were from the Gibbs Sea-Water Oceanographic Toolbox available at http://www.teos-10.org/software.htm#1. Code which implements the methods described in the Methods Section are available at dropbox.com/sh/wl1ry8lbf6m56mv/AABIbWi5blAucyzEQQWXF2oVa?dl=0 and will be made available in a stable online repository before publication. The aforementioned code includes FastEMD (Pele and Werman 2008, 2009) software available at http://www.cs.huji.ac.il/ ofirpele/FastEMD/.

APPENDIX

Accuracy of the warming estimates we have produced rely on the following assumptions:

1. The mapping from transformations in $T-S$ space for each region to local changes in geographical space is accurate;
2. The 'minimum transformation' inferred using the EMD algorithm, including our choice of distance metric, accurately estimates the net thermodynamic transformation;
3. The resolution of our T-S grid is sufficiently fine to capture relevant water masses; and
4. The density of observations and the procedure used to map them onto a regular grid is sufficiently accurate for us to quantify changes in water mass volumes.

We investigate the impact of each of these assumptions in the supplementary text. We investigate 1 and 2 using synthetic data from a climate model where 'added heat' is explicitly simulated (Section 1) and we investigate 3 and 4 using sensitivity tests (Section 2 and Section 3). A bootstrap approach is taken in the latter case to derive uncertainty estimates.

A1. Validation using synthetic data

We use synthetic data from the Hadley Centre Climate Model version HadCM3 (Gordon et al. 2000) to validate the method described in the methods section. Specifically, we exploit the configuration used for the Flux Anomaly Forced Model Inter-comparison Project (FAFMIP, Gregory et al. 2016). We will consider two specific model experiments used by FAFMIP: $piControl$, which is a reference experiment with no external forcing, and $FAFheat$, where the ocean is warmed by an imposed surface heat flux.

In $FAFheat$ 'added temperature' (T_{added}) and 'redistributed temperature' (T_{redist}) tracers are simulated explicitly. T_{added} is simulated as a passive tracer initialized at zero and forced at the ocean boundary by the imposed heat flux anomaly. T_{redist} is simulated, again, as a passive tracer,

which is initialized with the true ocean temperature at the start of the perturbation experiment and does not increase with the imposed heat flux anomaly but continues to respond to all other fluxes of heat at the sea surface within the coupled climate model. By construction the T in $FAFheat$ is the sum of the T_{added} and T_{redist}. Unlike the redistributed heat inferred using our method, T_{redist} can be a net non-zero contributor to ocean heat content. This is because in both $piControl$ and $FAFheat$ the surface heat flux can vary because of unforced fluctuations which are not constrained to sum to zero, and in $FAFheat$ it is modified also due to changes in sea surface temperature, caused by changes in ocean circulation, arising from buoyancy forcing by the imposed heat perturbation. For more details of this phenomenon and of FAFMIP in general see Gregory et al. (2016).

There are two aspects of our method which we aim to validate using these data: the uncertainty introduced by 1) projecting an inferred warming signal from temperature and salinity classes (water masses) to the geographical location of those water masses and 2) using the Earth Mover Distance Algorithm.

The FAFMIP protocol does not describe historical climate change but rather an idealized increase in ocean heat content as would be expected from a doubling in atmospheric CO2. Our observational record is centered on the beginning of 2012 when the global atmospheric CO2 concentration reached 392 parts per million (Conway et al. 1994), which is approximately 40% above pre-industrial levels of approximately 280 parts per million. Although no comparison can be perfect, we consider this reasonable motivation to choose years 35-46 of the FAFMIP experiments to test our method.

HadCM3 conserves potential temperature and a salinity variable initialized based on observed practical salinity, so we use these to define temperature and salinity respectively for the purposes of defining water masses in this analysis.

a. Validation of the water mass based projection

Fig. A4 a shows the column integral of the added heat tracer for years 41 to 46 for the HadCM3 $FAFheat$ experiment (the tracer is represented in Kelvin but is here converted to more familiar W/m2 by multiplying by the heat capacity and density and dividing by 43 years). As was done to the EN4 data, we selected water mass bins using a quadtree approach. Fig. A4b shows column integrated added heat change between years 41-46, but in this case where the added heat tracer is first averaged within each water mass within each of the 9 geographical regions, then projected back into the location of those water masses. What this projection amounts to is simply homogenizing the added heat tracer within each water mass in each region. If added heat change varies substantially within a water mass this method will smooth out those variations. In the zonal mean (Fig. A4c) the re-projected added heat has an RMS error of 0.5 TW/°lat.

b. Validation of the Earth Mover Distance based method

We will test our method in the following three scenarios:

1. Added heat only - heat is added to the ocean and water masses are not redistributed;

2. Redistribution only – no heat is added and water masses are redistributed;

3. Added and redistributed heat – Heat is added and water masses are redistributed.

Table A1 details the way data from $piControl$ and $FAFheat$ are used for these scenarios.

1) Scenario 1

In this scenario there is no explicit 'redistribution' signal in the model data. The purpose of this validation is to see how much of the change is attributed to material heat content change using our water mass change approach. In the zonal mean (Fig. A4A) the difference between the simulated

and inferred added heat (which is precisely the inferred redistributed heat) has an RMS of 1.8 TW/°lat.

2) Scenario 2

In this scenario there is no explicit 'added heat' signal in the model data. This is simply a climate control run with no variations in forcing (solar, aerosol etc). There is, however, some very small changes in ocean heat uptake due to natural variability in the fluxes of heat at the air-sea interface. The purpose of this validation is to see how much of the change is attributed to our redistributed heat using our water mass change approach. In the zonal mean (Fig. A4B) the difference between the simulated heat content change and the inferred redistributed heat (which is precisely the inferred added heat) has an RMS of 0.4 TW/°lat.

3) Scenario 3

In this scenario there is both an explicit 'added heat' signal in the model data and the model redistributes heat in response to both natural variability and the imposed warming. Despite the inclusion of a non-zero global mean net surface heat flux in FAFMIP redistributed heat (as described above), it is instructive to see how well our material and redistributed heat estimates compare to the directly simulated added and redistributed heat variables. In the zonal mean (Fig. A4C) the difference between both the simulated FAFMIP added heat content and the inferred material heat content change and between the simulated FAFMIP redistributed heat and our water mass based redistributed heat, has an RMS of 2.4 TW/°lat. We emphasize that this difference should not necessarily be directly attributed to an inaccuracy in our method considering the differing meanings of redistributed heat between the model simulations and our method. Broadly we consider the stated differences between directly simulated and inferred changes to be acceptable. We made no

attempt to tune method parameters to optimize correspondence with the simulated variables, but this could be pursued in future.

A2. Parameter sensitivity

Here we test the sensitivity of the results, in particular the zonally integrated added heat, to parameter choices within the water mass method.

The two choices were: i) the choice of relative penalty on temperature versus salinity changes (i.e. parameter 'a') and ii) the number of water masses in T-S space used to represent the early and late ocean states. We discuss sensitivity to these choices here.

The reference case for a is the ratio of a constant haline contraction coefficient (β_0 =7.55 x 10-4 kg/ (g/kg) m^3) to a constant thermal expansion coefficient (α_0 = 1.76 x 10-4 kg/ K m^3; i.e. $a_0 = \alpha_0/\beta_0$ = 4.3K / (g / kg)). This choice implies a transformation by 1g/kg in absolute salinity is penalized equivalently to a transformation of 4.3K in temperature. A larger a will cause the method to favor transformation along the S axis and a smaller a will favor transformation along the T axis. We test the method in the following cases: $a = a_0$; $a_0/2$ and $2*a_0$ (Fig. A4A) and find RMS differences of 0.3 TW / °lat between the reference case and the doubling and halving cases.

In terms of $T - S$ resolution, our reference case has a minimum $T - S$ bin size of 0.2 g / kg and 0.4 K. Using the quadtree method the grid is refined until either this resolution is achieved or the volume within a particular bin falls below 62×10^{12} m^3. We test the sensitivity of this choice by both refining and coarsening the resolution by a factor of two in both the salinity and temperature dimensions and reducing the volume threshold by a factor of four also.

Decreasing the resolution induces an RMS change in estimated zonally averaged OHC of 0.5 TW/°lat and increasing the resolution induces an RMS change of 0.4 TW/°lat (Fig. A4B).

A3. Robustness of 21st Century trend

To quantify the sensitivity of our trend results to the time period chosen and the specific observations made and mapped in that period, we carry out a bootstrap calculation. Our aim here is not to determine how accurate our trend is, but rather to determine how representative it is of time period as a whole or if specific years strongly influence the result.

We chose to subsample the data by including and excluding entire years from the analysis. Six years are used for the early (2006-2011) and late (2012-2017) periods of our analysis of EN4. We therefore considered all possible permutations of the numbers one to six and re-ran our analysis of EN4 subsampling the years corresponding to those six numbers. For example, in the case [1, 3, 3, 4, 5, 6] the 'early period' data was replaced with the years 2006, 2008 repeated twice, 2009, 2010 and 2011 and the 'late period' with 2012, 2014 repeated twice, 2015, 2016 and 2017.

There are 46656 uniquely ordered permutations of the numbers one to six when repetition is permitted. Since the calculation is insensitive to the order of the six years for either the early or late period, in practice we only need to consider the 462 unique permutations (ignoring order) and weight each by its frequency in the larger set of ordered permutations.

Fig. 3 shows the mean while Fig. A4 shows the standard deviation of the bootstrap ensemble. Plus and minus two standard deviations of the spread in estimates of zonally averaged heat content change are shown in Fig. 4. Since these error estimates are generally larger than our other parameter sensitivity tests, we use them as our formal uncertainties throughout the main text.

A4. Comparison with Atlantic meridional heat transport trend at 26°N

We will compare our estimate of the contribution of redistribution to MHT north of 26°N in the Atlantic (Fig. 4C) with data reported by Bryden et al. (2020) (Tab. A4). MHT relates to the rate of change of OHC. That is $MHT = \partial OHT/\partial t$. The difference in OHC between two year (for example

2006 and 2012) relates to MHT via

$$\int_{2006}^{2012} MHT\,dt = OHC(2012) - OHC(2006). \tag{A1}$$

We have considered the difference in OHC between two 6 year periods (2006-2011 versus 2012-2017). Hence our OHC change and MHT are related via

$$\left(\int_{t_0}^{t_0+\Delta t} \mathrm{OHC}(t)dt - \int_{t_0-\Delta t}^{t_0} \mathrm{OHC}(t)dt\right) = \int_{t_0}^{t_0+\Delta t} (\mathrm{OHC}(t) - \mathrm{OHC}(t-\Delta t))\,dt = \int_{t_0}^{t_0+\Delta t}\int_{t-\Delta t}^{t} \mathrm{MHT}(t')dt'dt \tag{A2}$$

where t_0 is midnight on the 31st December 2012 and Δt is 6 years. In practice we have averages of MHT covering April-March (see table A4), we approximate (A2) using 6 year running means of MHT then averaging these between 2009-2010 and 2014-2015. Our uncertainties are ± two times the standard deviation of the 6-year running means.

References

Banks, H. T., and J. M. Gregory, 2006: Mechanisms of ocean heat uptake in a coupled climate model and the implications for tracer based predictions of ocean heat uptake. *Geophysical Research Letters*, **33 (7)**.

Bindoff, N. L., and T. J. McDougall, 1994: Diagnosing climate change and ocean ventilation using hydrographic data. *Journal of Physical Oceanography*, **24**, 1137–1152.

Bryden, H. L., W. E. Johns, B. A. King, G. McCarthy, E. L. McDonagh, B. I. Moat, and D. A. Smeed, 2020: Reduction in ocean heat transport at 26°n since 2008 cools the eastern subpolar gyre of the north atlantic ocean. *Journal of Climate*, **33 (5)**, 1677–1689.

Church, J., and Coauthors, 2013: *Sea Level Change*, book section 13, 1137–1216. Cambridge University Press, Cambridge, United Kingdom and New York, NY, USA, doi: 10.1017/CBO9781107415324.026, URL www.climatechange2013.org.

Conway, T. J., P. P. Tans, L. S. Waterman, K. W. Thoning, D. R. Kitzis, K. A. Masarie, and N. Zhang, 1994: Evidence for interannual variability of the carbon cycle from the national oceanic and atmospheric administration/climate monitoring and diagnostics laboratory global air sampling network. *Journal of Geophysical Research: Atmospheres*, **99 (D11)**, 22 831–22 855.

Döös, K., J. Nilsson, J. Nycander, L. Brodeau, and M. Ballarotta, 2012: The World Ocean Thermohaline Circulation. *Journal of Physical Oceanography*, **42**, 1445–1460.

Drijfhout, S. S., A. T. Blaker, S. A. Josey, A. Nurser, B. Sinha, and M. Balmaseda, 2014: Surface warming hiatus caused by increased heat uptake across multiple ocean basins. *Geophysical Research Letters*, **41 (22)**, 7868–7874.

Evans, D. G., J. Toole, G. Forget, J. D. Zika, A. C. Naveira Garabato, A. G. Nurser, and L. Yu, 2017: Recent wind-driven variability in atlantic water mass distribution and meridional overturning circulation. *Journal of Physical Oceanography*, **47 (3)**, 633–647.

Evans, D. G., J. D. Zika, A. C. Naveira Garabato, and A. Nurser, 2014: The imprint of southern ocean overturning on seasonal water mass variability in drake passage. *Journal of Geophysical Research: Oceans*, **119 (11)**, 7987–8010.

Evans, D. G., J. D. Zika, A. C. Naveira Garabato, and A. G. Nurser, 2018: The cold transit of southern ocean upwelling. *Geophysical Research Letters*, **45 (24)**, 13–386.

Good, S. A., M. J. Martin, and N. A. Rayner, 2013: EN4: Quality controlled ocean temperature and salinity profiles and monthly objective analyses with uncertainty estimates. *Journal of Geophysical Research: Oceans*, **118 (12)**, 6704–6716.

Gordon, C., C. Cooper, C. A. Senior, H. Banks, J. M. Gregory, T. C. Johns, J. F. Mitchell, and R. A. Wood, 2000: The simulation of sst, sea ice extents and ocean heat transports in a version of the hadley centre coupled model without flux adjustments. *Climate dynamics*, **16 (2-3)**, 147–168.

Gregory, J. M., and Coauthors, 2016: The flux-anomaly-forced model intercomparison project (FAFMIP) contribution to CMIP6: investigation of sea-level and ocean climate change in response to CO_2 forcing. *Geoscientific Model Development*, **9 (11)**, 3993.

Griffies, S. M., and Coauthors, 2009: Coordinated Ocean-ice Reference Experiments (COREs). *Ocean Modelling*, **26**, 1–46.

Groeskamp, S., S. M. Griffies, D. Iudicone, R. Marsh, A. G. Nurser, and J. D. Zika, 2019: The water mass transformation framework for ocean physics and biogeochemistry. *Annual review of marine science*, **11**, 271–305.

Groeskamp, S., J. D. Zika, T. J. McDougall, B. M. Sloyan, and F. Laliberté, 2014: The representation of ocean circulation and variability in thermodynamic coordinates. *Journal of Physical Oceanography*, **44 (7)**, 1735–1750.

Hieronymus, M., J. Nilsson, and J. Nycander, 2014: Water mass transformation in salinity–temperature space. *Journal of Physical Oceanography*, **44 (9)**, 2547–2568.

Khatiwala, S. P., and Coauthors, 2013: Global ocean storage of anthropogenic carbon. *Biogeosciences*, **10 (4)**, 2169–2191.

Kuhlbrodt, T., and J. M. Gregory, 2012: Ocean heat uptake and its consequences for the magnitude of sea level rise and climate change. *Geophysical Research Letters*, **39 (18)**, L18 608.

Lee, S.-K., W. Park, E. van Sebille, M. O. Baringer, C. Wang, D. B. Enfield, S. G. Yeager, and B. P. Kirtman, 2011: What caused the significant increase in atlantic ocean heat content since the mid-20th century? *Geophysical Research Letters*, **38 (17)**.

Maximenko, N., P. Niiler, L. Centurioni, M.-H. Rio, O. Melnichenko, D. Chambers, V. Zlotnicki, and B. Galperin, 2009: Mean dynamic topography of the ocean derived from satellite and drifting buoy data using three different techniques. *Journal of Atmospheric and Oceanic Technology*, **26 (9)**, 1910–1919.

Montgomery, R. B., 1958: Water characteristics of atlantic ocean and of world ocean. *Deep Sea Research (1953)*, **5 (2-4)**, 134–148.

Nycander, J., J. Nilsson, K. Döös, and G. Bromström, 2007: Thermodynamic analysis of Ocean Circulation. *Journal of Physical Oceanography*, **37**, 2038–2052.

Palmer, M. D., and K. Haines, 2009: Estimating oceanic heat content change using isotherms. *Journal of Climate*, **22 (19)**, 4953–4969.

Pele, O., and M. Werman, 2008: A linear time histogram metric for improved sift matching. *European conference on computer vision*, Springer, 495–508.

Pele, O., and M. Werman, 2009: Fast and robust earth mover's distances. *2009 IEEE 12th International Conference on Computer Vision*, IEEE, 460–467.

Penduff, T., M. E. Juza, B. Barnier, J. D. Zika, W. K. Dewarr, A.-M. Treguier, J.-M. Molines, and N. Audiffren, 2011: Sea Level Expression of Intrinsic and Forced Ocean Variabilities at Interannual Time Scales. *Journal of Climate*, **24**, 5652–5670.

Rhein, M., and Coauthors, 2013: Observations: ocean.

Roberts, C. D., M. D. Palmer, R. P. Allan, D. G. Desbruyeres, P. Hyder, C. Liu, and D. Smith, 2017: Surface flux and ocean heat transport convergence contributions to seasonal and interannual variations of ocean heat content. *Journal of Geophysical Research: Oceans*, **122 (1)**, 726–744.

Roemmich, D., and J. Gilson, 2011: The global ocean imprint of enso. *Geophysical Research Letters*, **38 (13)**.

Smeed, D., and Coauthors, 2013: Observed decline of the atlantic meridional overturning circulation 2004 to 2012. *Ocean Science Discussions*, **10 (5)**, 1619–1645.

Walin, G., 1982: On the relation between sea–surface heat flow and thermal circulation in the ocean. *Tellus*, **34**, 187–195.

Zanna, L., S. Khatiwala, J. M. Gregory, J. Ison, and P. Heimbach, 2019: Global reconstruction of historical ocean heat storage and transport. *Proceedings of the National Academy of Sciences*, **116 (4)**, 1126–1131.

Zhang, X., and J. A. Church, 2012: Sea level trends, interannual and decadal variability in the pacific ocean. *Geophysical Research Letters*, **39 (21)**.

Zika, J. D., M. H. England, and W. P. Sijp, 2012: The Ocean Circulation in Thermohaline Coordinates. *Journal of Physical Oceanography*, **2**, 708–724, doi:10.1175/JPO-D-11-0139.1.

Zika, J. D., F. Laliberté, L. R. Mudryk, W. P. Sijp, and A. Nurser, 2015a: Changes in ocean vertical heat transport with global warming. *Geophysical Research Letters*, **42 (12)**, 4940–4948.

Zika, J. D., N. Skliris, A. G. Nurser, S. A. Josey, L. Mudryk, F. Laliberté, and R. Marsh, 2015b: Maintenance and broadening of the ocean's salinity distribution by the water cycle. *Journal of Climate*, **28 (24)**, 9550–9560.

LIST OF TABLES

584 TABLE 1. Heat content change by ocean basin in TW. Estimates are based on differences between the periods
585 2006-2011 and 2012-2017 inclusive. Uncertainties are ± two standard deviations. The Southern Ocean is defined
586 as the entire ocean south of 32°S. The South Pacific, South Atlantic and Indian Ocean estimates exclude the
587 ocean south of 32°S. The North Atlantic is split into a region south and a region north of 44°N. The later includes
588 the Arctic Ocean.

	Material	Redistributed	Total
Southern Ocean	90 ± 18	118 ± 50	208 ± 63
South Pacific	53 ± 16	-26 ± 22	28 ± 22
North Pacific	82 ± 25	-61 ± 55	21 ± 54
Indian Ocean	45 ± 10	-13 ± 25	32 ± 30
South Atlantic	34 ± 11	6 ± 7	40 ± 7
North Atlantic (< 44°N)	75 ±33	20 ± 17	95 ± 46
North Atlantic (> 44°N)	19 ± 6	-40 ± 13	-20 ± 16
Global Ocean	398 ± 81	0	398 ± 81

589 Table A1. Summary of data used for three validation scenarios. T_{ref} and S_{ref} are the temperatures and
590 salinities from the $piControl$ experiment respectively. T_{added} is the added heat variable and T_{redist} is the
591 redistributed heat variable from the $FAFheat$ experiment. S_{heat} is the salinity variable from the $FAFheat$
592 experiment. The numbers in brackets are the experiment years chosen (e.g. T_{ref}(41-46) is temperature from
593 years 41 to 46 of the piControl experiment).

Scenario	Early period	Late period
1	T = T_{ref}(41-46),	T = T_{ref}(41-46)+T_{added}(41 − 46)
	S = S_{ref}(41-46)	S = S_{ref}(41-46)
2	T = T_{ref}(35-40)	T = T_{ref}(41-46)
	S = S_{ref}(35-40)	S = S_{ref}(41-46)
3	T = T_{added}(35-40)+T_{redist}(35-40)	T = T_{added}(41-46)+T_{redist}(41-46)
	S = S_{ref}(35-40)	S = S_{heat}(41-46)

594

595 Table A2. Atlantic meridional heat transport (MHT, in PW) at 26°N (Bryden et al. 2020), MHT anomaly
596 relative to 2006-2017 and 6-year running mean MHT. The mean of 6-year running means is relevant to the
597 difference in OHC between 2006-2011 and 2012-2017.

Year	MHT	Anomaly	6-year mean
2006-2007	1.37	0.178	-
2007-2008	1.3	0.108	-
2008-2009	1.23	0.038	-
2009-2010	0.91	-0.282	0.018
2010-2011	1.19	-0.002	-0.038
2011-2012	1.26	0.068	-0.043
2012-2013	1.03	-0.162	-0.057
2013-2014	1.27	0.078	-0.011
2014-2015	1.15	-0.042	-0.007
2015-2016	1.18	-0.012	-
2016-2017	1.22	0.028	-
		Mean	-0.023
		Std	0.029

598

LIST OF FIGURES

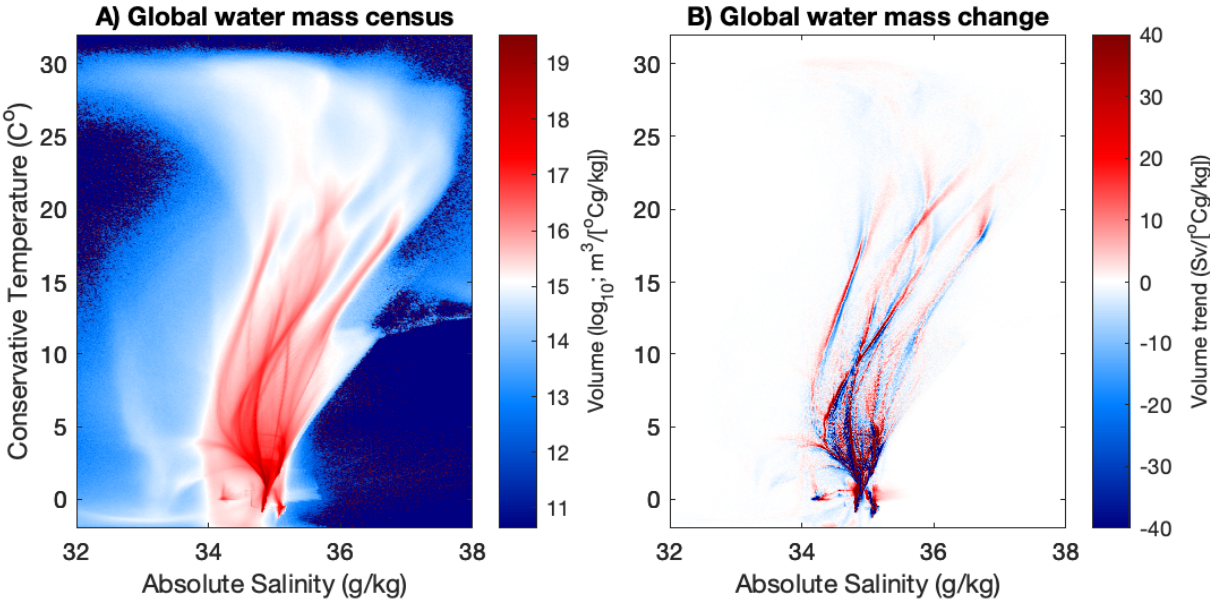

FIG. 1. Portrait of changing ocean water masses. A: Inventory of ocean volume in conservative temperature versus absolute salinity coordinates (mean of 2006 to 2017 inclusive). B: Change in water mass volume between the early half and late half of the period divided by the six years (Sv = 106m3/s). According to water mass theory, changes in air-sea heat and fresh water fluxes and/or changes in rates of diffusion are required for these changes to occur.

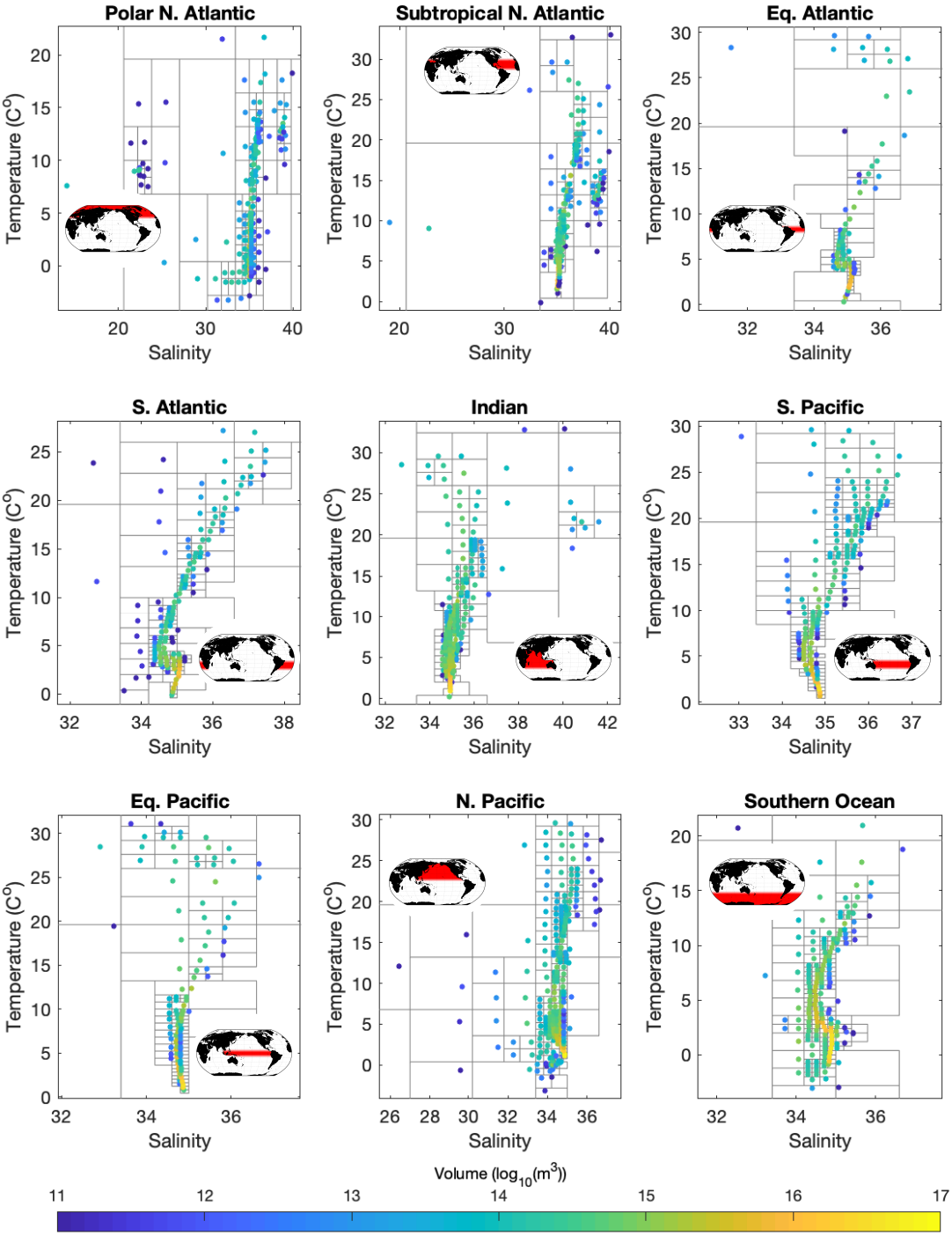

FIG. 2. Grey lines show conservative temperature, T, and absolute salinity, S, bounds of each water mass (or 'bin') generated by the quadtree method for each geographical region. The average T and S of the water found within each bin is shown by the location of each marker and the volume is represented by the color scale ($\log_{10}(\mathrm{m}^3)$). Inventories and mean T and S values represent the entire period (2006-2017 inclusive). Inset panels show masks associated with each geographical region.

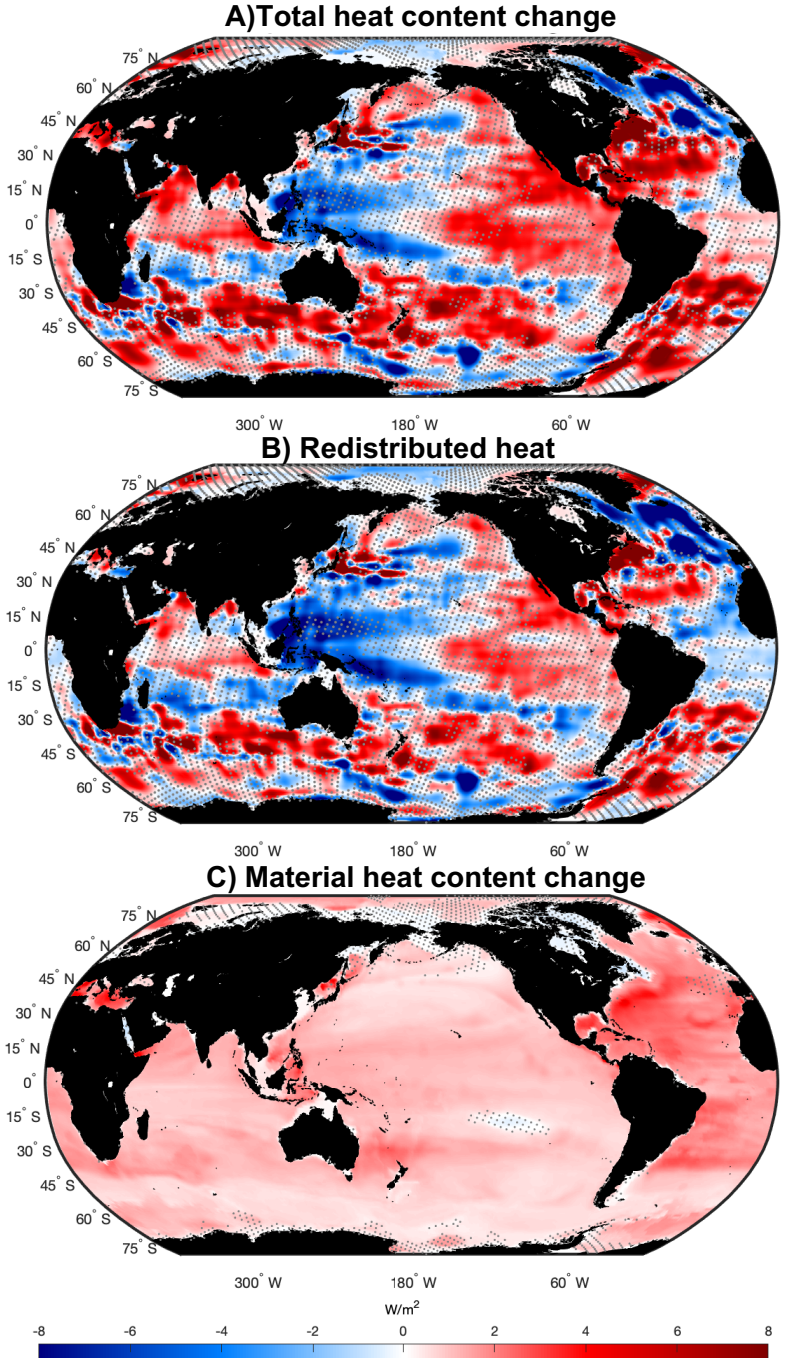

FIG. 3. Heterogeneous pattern of total and redistributed heat content change contrast against robust material heat content change. A: Change in depth integrated ocean heat content between years 2006-2011 and 2012-2017 inclusive. B: Inferred redistributed heat and C: Inferred material heat content change based on changing water masses for the same period. Regions where the magnitude of the signal is less significant (less than two standard deviations of a bootstrap ensemble) are stippled.

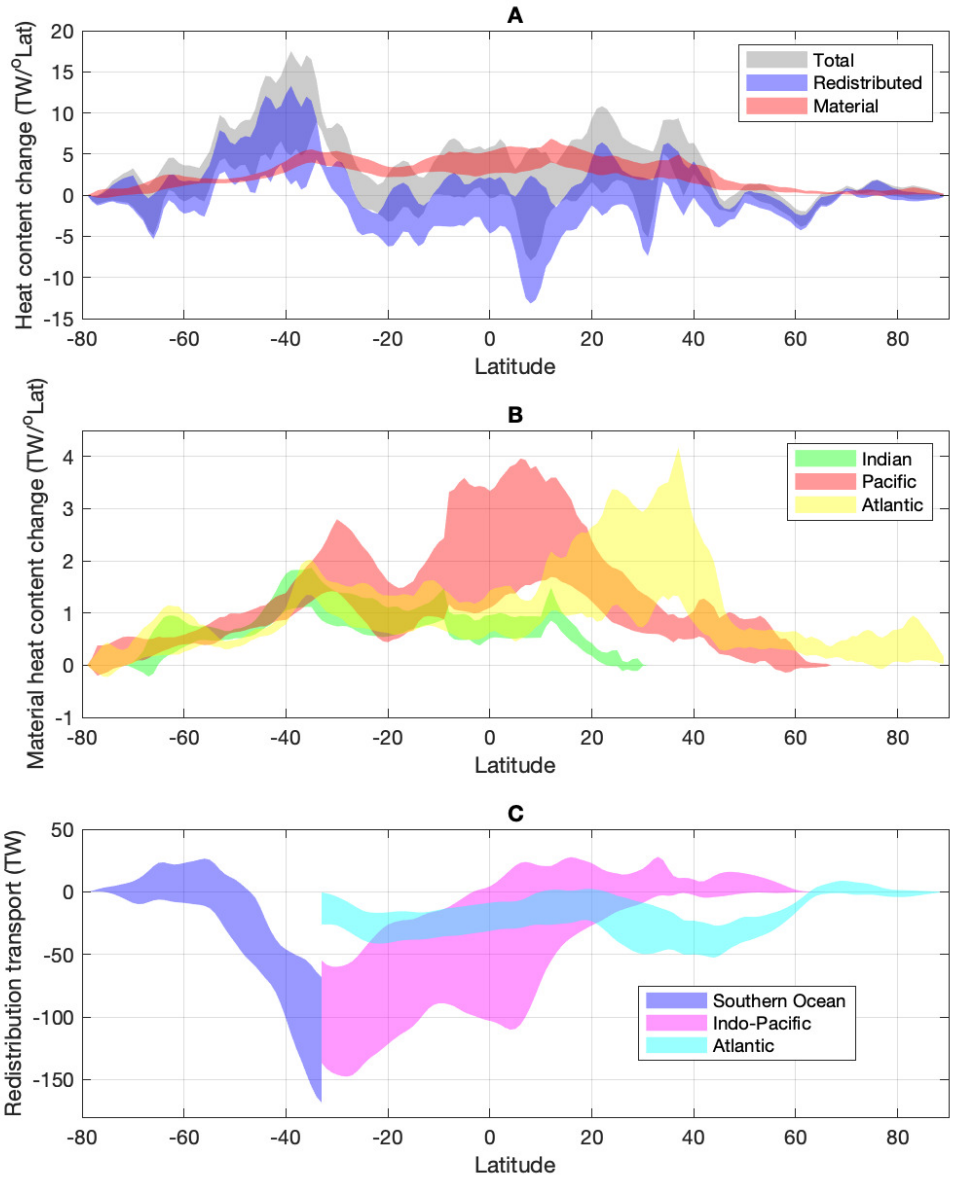

FIG. 4. Material heat content change is accumulating in the tropics and sub-tropics existing heat is being redistributed southward. A: Total heat content change (grey) redistribution contribution (blue) and material contribution (red). B: Contributions to material heat content change from the Indian (green), Pacific (orange) and Atlantic (yellow) Oceans. C: Meridional heat transport due to redistribution in the Southern Ocean (blue), Atlantic (cyan) and Indian plus Pacific Oceans (magenta). Estimates are bootstrap ensemble means with shading representing ± two standard deviations.

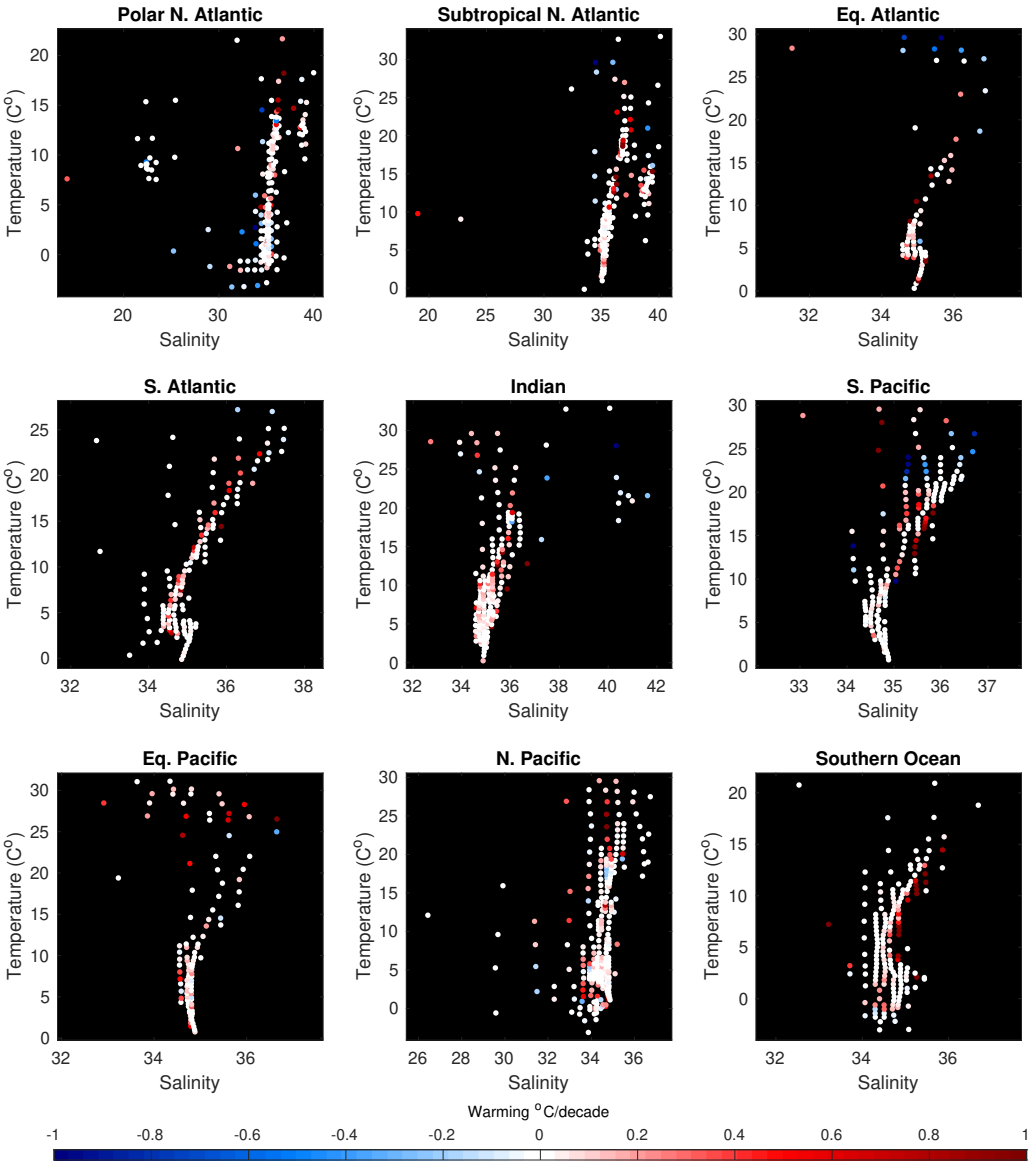

672 Fig. S1. Each marker shows $\Delta T_{material}$, the average warming required for each early water mass in order to
673 transform them into the set of late water masses.

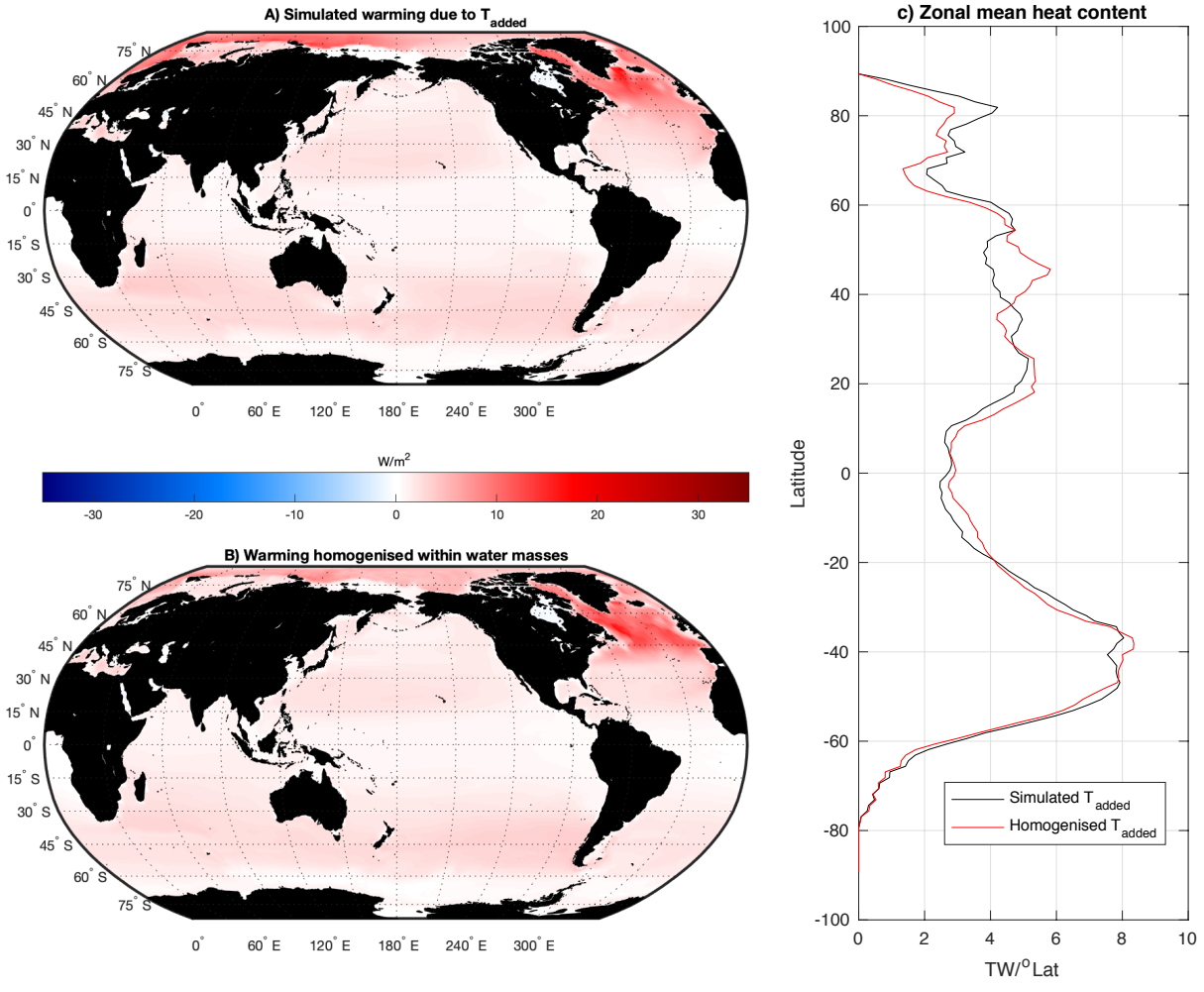

Fig. S2. A: Directly simulated added heat by the FAFheat experiment averaged over years 41-46 of the experiment. B: Inferred added heat when the same FAFheat data is first homogenized in water masses (bins in temperature-salinity coordinates) then remapped into the locations of those water masses over the same period. C: Comparison of the zonal integration of the two quantities shown in A and B.

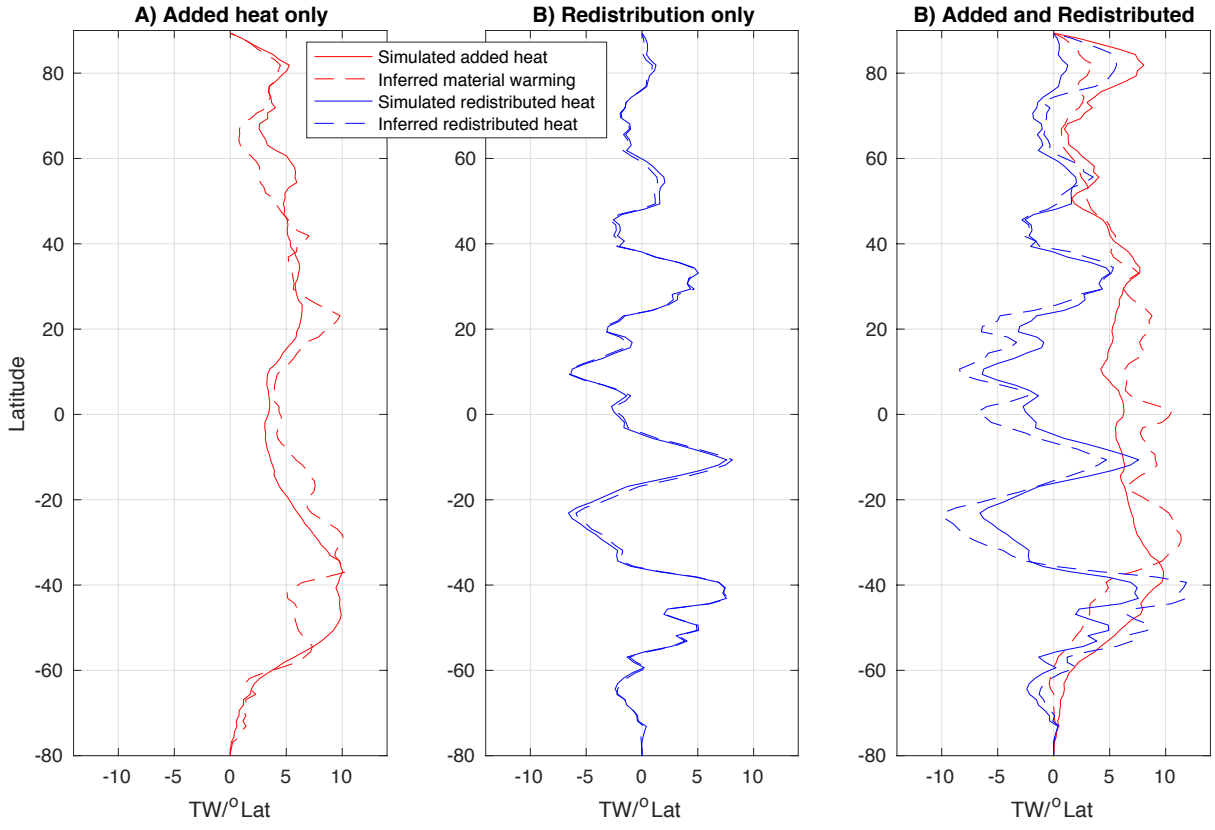

Fig. S3. A: Zonally integrated simulated added heat (solid, red) and inferred material heat content change (dashed, red) based on our water mass method for years 41-46 of the $FAFheat$ experiment comparing the simulation with and without added heat. B: Zonally integrated simulated heat content change (solid, blue) and inferred redistributed heat (dashed, blue) based on our water mass method comparing years 35-40 and 41-46 of the $piControl$ experiment. C: Zonally integrated simulated added heat (solid, red) and redistributed heat (blue, solid) in the $FAFheat$ experiment and inferred material heat content change (dashed, red) and redistributed heat (dashed, blue) based on our water mass method applied the model data.

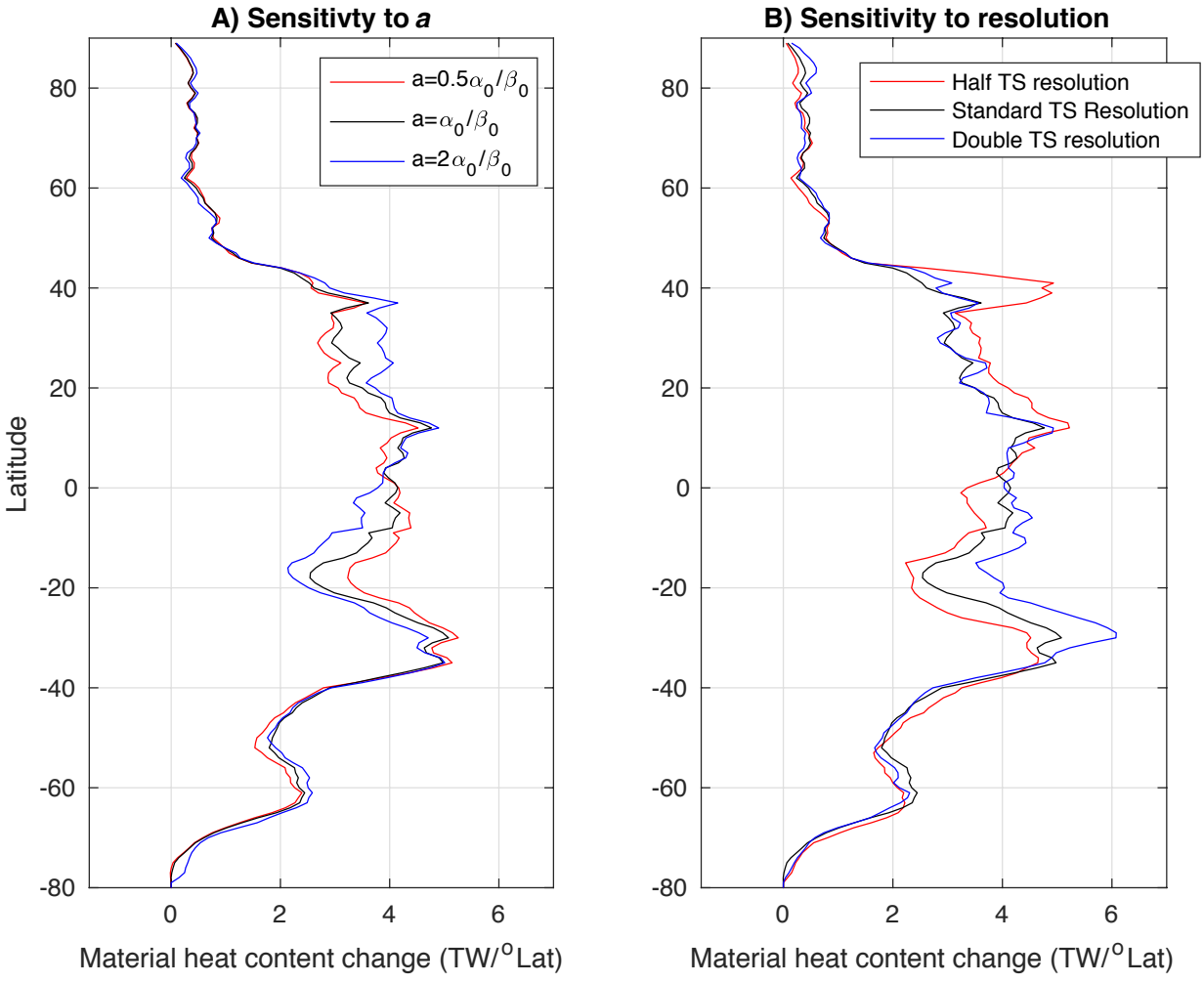

Fig. S4. A: Zonally integrated inferred material heat content change for cases where the parameter a is set at a reference value of $a_0=\alpha_0/\beta_0$ = 4.3K/(g/kg) (black) and then reduced (red) and increased (blue) by a factor of two. B: Zonally integrated inferred material heat content change for cases where the $T-S$ bins are shrunk using a quadtree method until they either contain a volume of sea water less than 62 x 1012m3 or have a bin size of 0.4^{o}C by 0.2 g/kg (black). Cases where the minimum volume is 15.5 x 1012 m^3 and the minimum bin size is 0.2^{o}C by 0.1g/kg (blue) and where the minimum volume is 248 x 1012 m^3 and the minimum bin size is 0.8°C by 0.4g/kg (red).

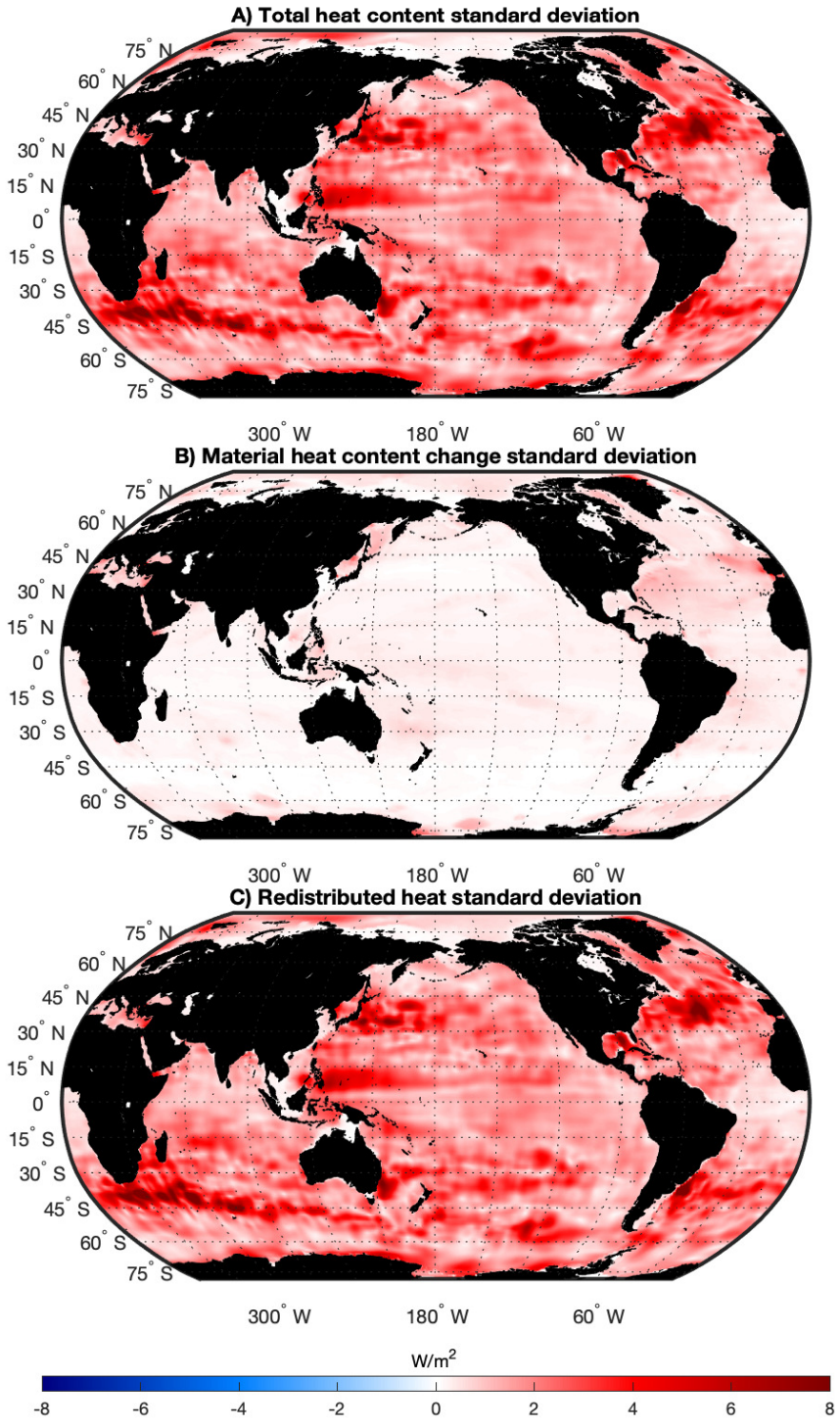

692 Fig. S5. A: One standard deviation of the heat content change inferred based on subsampling 'early' and 'late'
693 years of the EN4 data set. One standard deviation of the ensemble of inferred material heat content change (B)
694 and redistributed heat (C) based on our water mass method applied to the same subsampled data as in A.